ANNALS OF GEOPHYSICS, 62, 2, VO216, 2019; doi: 10.4401/ag-7859

APPENDICES TO: ADVANCES IN THE RHEOLOGY OF NATURAL MULTIPHASE SILICATE MELTS: IMPORTANCE FOR MAGMA TRANSPORT AND LAVA FLOW EMPLACEMENT

APPENDIX A1. SHORT REVIEW OF SOME OF THE MOST COMMON METHODS TO MEASURE VISCOSITY.

The basic nature of magmas and volcanic products changes from liquids, through foams, emulsions, crystal suspensions, and partially molten aggregates. The rheology of such widely varying materials, each complex in its own right, and the fact that the viscosity of these materials can span over, at least, 16 orders of magnitude, defies the use of one single method to fully characterize their behavior. A large variety of devices for the measurement of the deformation and transport behavior of magmas, lavas and others volcanic materials have been presented in literature to date and this continuously evolving field produces novel techniques on a regular basis. These range from new devices for laboratory measurements to novel methods for ground- and satellite-based viscosity estimates. This field is growing in order to accomplish the complex task of defining the rheology of natural systems or analogues.

In principle, viscosity information of a material can be obtained from any data where time evolution of strain ($\gamma = (dx/dz)$) and strain-rate $\left(\dot{\gamma} = d\gamma/dt = 1/dt\ (dx/dz)\right)$ in response to an applied stress (σ) can be recorded.

Viscometry can therefore be performed in devices where either strain-rate is maintained constant while the resulting stress is measured (e.g., concentric cylinder) or when the imposed stress

is kept constant and the resulting strain-rate is measured [e.g., micropenetration and fiber elongation; Dingwell et al., 1993]. For the sake of brevity, I will not report the details and analytical procedure of each experimental device here but rather I will provide the most relevant reference papers describing the devices and the experimental procedures in detail.

Experimental efforts are to date largely subdivided into two categories of two phase suspension rheometry, namely i) those measuring volatile-bearing suspensions and, ii) those measuring particle bearing suspensions where volatiles cannot be retained dissolved in the liquid phase at experimental conditions. At room temperature conditions this distinction fundamentally identifies two temperature intervals: i) low-temperature experiments, at or close to the glass transition temperature, where volatile dissolution kinetics and, in most cases, crystals formation processes are slow enough not to allow gas exsolution and crystal formation during the experiment (these span viscosities in the range between ~ 10^8 to 10^{12}) and, ii) the high-temperature experiments, where pure liquid and liquid+crystals measurements can be performed. A small number of laboratory studies of viscous deformation of volatile plus crystal-bearing mixtures at high pressure and temperature also exist. The main advantage of these apparata is that, in some case, they attain P-T conditions more realistic for geologically relevant multiphase assemblages and they allow measurements on volatile bearing liquids at superliquidus conditions.

A1.1. ROTATIONAL (COUETTE) RHEOMETRY

The advantage of the rotational concentric cylinder viscometry, compared to other viscometers, is the possibility to operate continuously at given conditions (e.g. shear rate or shear stress), so that steady-state measurements can performed while systematically varying the experimental conditions. This allows detecting and quantifying any time dependency of the viscosity of the studied material via measurement at different deformation regimes and geometries and during temperature variation. Therefore, rotational viscometers are among the most widely used devices for measurements on magma rheology. The most common type are Couette-flow Searle type

viscometers, where the inner cylinder rotates (at constant strain-rate or stress). The sample is deformed in an annulus of liquid filling the gap between a rotating inner spindle (commonly a cylinder, or a cone-plate geometry) and an outer cylindrical cup. Rheometry on natural silicate melts is commonly performed in both a wide gap or small gap geometry (depending also on the viscosity value), where, some time, the velocity profile across the deforming liquid or suspension is non-linear. As such, determination of the sample viscosity relies on calibration of the measured torque against well characterized standard materials for which the temperature viscosity relationship is accurately known.

Viscosities are calculated from the equation for Newtonian liquids:

$$\eta = \frac{M}{4 \cdot \pi \cdot \Omega \cdot (l)} \left(\frac{1}{r^2} - \frac{1}{R^2} \right) \qquad \text{(A1.1)}$$

where M is the torque, Ω is the angular velocity of the outer cylinder, r and R are the respective radii of the inner and outer cylinders, and (l) is the effective length of the inner cylinder.

As above mentioned, the common approach for natural silicate melt viscometry at high temperature is to use a wide gap geometry and calibrating the torque exerted on a spindle to the melt viscosity using a standard. As it can be retrieved by Eq. A1.1 wide gap geometry has the disadvantage of being slightly less accurate than small gap geometry, but the advantage of introducing small viscosity reading errors in the case of crystallization on the adopted rotating spindles or in the gap space.

Early devices of this type that produced a plethora of experimental data are described in a series of papers measuring the viscosity of synthetic silicate melts [Dingwell 1986; Dingwell 1989; Dingwell and Virgo 1988]. For these high temperature rheological experiments a solid precious metal spindle is hung from the measurement head and immersed into the sample while being rotated at a constant rate. In this setup, the torque needed to maintain a constant rotation rate is proportional to the melt/suspension viscosity and is recorded at a frequency of ~1 Hz. The spindles used in these

experiments vary in diameter and are chosen depending on the expected melt viscosity and rheological behaviour, to suit the torque and deformation rate range of interest. They are commonly machined to have a 45° conical top and bottom to reduce edge effects. Calibration of these devices is performed for shear-rates and temperatures exceeding those used in the experiments to account for mechanical effects in the measurement setup. The precision of the viscosity determination is ca. ±3% as described in Dingwell [1986]. Since direct temperature measurement inside the measuring crubile" after measurement during viscometry was not possible up until recently, the thermal evolution of the sample at the imposed temperatures is commonly calibrated over the entire experimental temperature range using a platinum sheathed type-S thermocouple immersed in an inert standard glass that does not crystallize over the entire calibration range.

The concentric cylinder (CC) technique is used to investigate both volatile-free liquids (at above liquidus conditions) and liquid+crystal suspensions (at subliquidus conditions) over the viscosity range between 10^{-1} and 10^{4} Pa s [Dingwell and Virgo, 1988; Chevrel et al. 2015; Chevrel et al. 2013a; Dingwell 1989; Dingwell and Virgo 1987; Giordano et al. 2005, 2007; Kolzenburg et al. 2016b; 2017; Sato 2005; Vetere et al. 2017; Vona et al. 2011, 2013]. CC viscometry has also been employed to study the effect of changing oxygen fugacity on melt and suspension viscosity via combination with gas mixing furnaces [see for example Dingwell and Virgo,1987, Chevrel et al., 2013a, Kolzenburg et al., 2018b].

There are two dominant mechanical constraints of these experimental apparatuses that inhibit rheometry at high viscosity values presented here 1) the torque limit of the rheometer head and 2) the fact that the crucible containing the experimental sample may start to slip and rotate in its holder at high torque, rendering the measured torque data useless. This issue was addressed recently in the construction of a new rheometer by Morgavi et al. [2015], who designed a new crucible-holder coupling, allowing both viscometry at higher torques, thus expanding the measure interval to 10^{6} Pa s, and allowing also for chaotic mixing experiments.

A further advancement in concentric cylinder viscometry at sub liquidus conditions was the development of an experimental device and method for in-situ differential thermal analysis during concentric cylinder rheometry as presented in Kolzenburg et al. [2016a]. This device allows tracking the change in the effective viscosity of the suspension due to crystallization as well as the latent heat released during crystallization. Such a device allowed studying the cooling-rate and the shear-rate dependence of sub liquidus lava rheology at conditions pertinent to lava flow emplacement [Kolzenburg et al., 2018c,d].

A1.2. DILATOMETRIC METHODS

These methods can be used to measure, at close to glass transition temperature (e.g. viscosity between 10^8 and 10^{14} Pa s), pure liquid as well as two-phase and three-phase suspensions (Robert et al., 2008a,b; Vona et al., 2013). The most widely used such devices are the dilatometric method of the micropenetration (Hess and Dingwell, 1986) and the uniaxial parallel plate (e.g. Robert et al., 2008a, b) the details of which are provided below.

Micropenetration

Micropenetration technique involves determining the rate at which an hemispherical Ir-indenter moves into the melt surface under a fixed load. The sample is placed in a silica rod sample holder under an Argon gas flow. The indenter is attached to one end of an alumina rod. The other end of the alumina rod is attached to a mass. The metal connection between the alumina rod and the weight pan acts as the core of a calibrated linear voltage displacement transducer (LVDT) [e.g. Hess and Dingwell, 1996]. The movement of this metal core as the indenter is pushed into the melt yields the displacement. The absolute shear viscosity is determined via the following equation [Pocklington, 1940; Tobolsky and Taylor, 1963]:

$$\eta\ (Pa \cdot s) = \frac{0.1875 \cdot P \cdot t}{r^{0.5} \cdot \alpha^{1.5}} \qquad \text{(A1.2)}$$

where P is the applied force, r is the radius of the hemisphere, t is the penetration time and α is the indentation distance. This provides an accurate viscosity value if the indentation distance is

lower than 150 – 200 microns. The technique allows viscosity to be determined at T up to 1100°C in the range $10^{8.5}$ to 10^{12} Pa·s without any problems with vesiculation. One advantage of the micropenetration technique is that it potentially only requires a small amounts of sample (other techniques used for high viscosity measurements, such as parallel plates and fiber elongation methods instead necessitate larger amount of material) if homogeneous pure liquids are to be measured.

Parallel plate

Using the parallel plate technique, the shear viscosity of the cores is computed for a given applied load (F; N), sample volume (V; m^3), sample length at time t (L; m), and rate of shortening ($\partial L/\partial t$; m/s) using the "no-slip" (Eq. A1.3), and "perfect-slip" (Eq. A1.4) models of Gent [1960] [cf. Dingwell et al. 1993]:

$$\eta_S\ (Pa \cdot s) = \frac{2\pi \cdot L^5 F}{3V \cdot \frac{dL}{dt}(2\pi L^3 + V)} \qquad \text{(A1.3)}$$

and

$$\eta_S\ (Pa \cdot s) = \frac{L^2 F}{3V \cdot \frac{dL}{dt}} \qquad \text{(A1.4)}$$

respectively. The "no slip" equation is used for the case in which the surface area of contact between the melt and the parallel plates remains constant and the cylinder bulges with increasing deformation. The "perfect slip" equation is used for the case in which the surface area between the cylinder and the measuring plate increases with deformation and the cylinder does not bulge.

A1.3. FALLING SPHERE METHOD (SIMPLE AND CENTRIFUGE)

The falling sphere method relies on determining the speed of a sphere (typically made of metal) falling through molten material. Viscosity is calculated according to the Stokes law as it follows:

$$\eta\ (Pa \cdot s) = \frac{2}{9} \cdot \frac{(\rho_S - \rho_M) \cdot a \cdot r^2}{v} \cdot C_F \qquad \text{(A1.5)}$$

where η is the viscosity (Pa·s), ρ_S-ρ_M the density contrast between the sinking sphere and the melt (kg/m3), a the acceleration of typically 1g (m/s^2), r the radius of the sphere (m), and v the velocity of the sinking sphere (m/s). C_F is the Faxèn correction term [Faxèn, 1922], which accounts for interactions between the sinking sphere and the wall of the capsule expressed by

$$C_F = 1 - 2.104 \cdot \left(\frac{r}{R}\right) + 2.09 \cdot \left(\frac{r}{R}\right)^3 - 0.95 \cdot \left(\frac{r}{R}\right)^5 \qquad \text{(A1.6)}$$

where R is the radius of the container, in which the sphere is positioned in the center. The Faxèn correction is considered to result in a slight underestimation of the calculated viscosity, but constitutes the best expression to account for the wall-effect on viscosity [Kahle et al., 2003].

Maximizing the density contrast (ρ_S - ρ_M) between the sphere and the melt reduces the uncertainty associated with the estimation of melt density. As a consequence Pt (ρ_S=21450 kg/m^3) or Mo spheres (ρ_S=10220 kg/m^3) are commonly employed.

Experiments that allow to investigate the variation of viscosity at the P-T-X(H_2O) conditions relevant to magmatic and volcanological environments are incredibly time consuming and require significant experimental effort. The range of viscosities investigated with the falling sphere technique varies from 10^{-4} Pa s [Brearley et al., 1986; Behrens and Schulze, 2003; Audetat and Keppler, 2004; Kanzaki et al., 1987; Taniguchi, 1995; Suzuki et al., 2005] to $10^{4.5}$ Pa s [Kushiro et al., 1976; Kushiro, 1976, 1977, 1978; Baker and Vaillancourt, 1995; Schulze et al., 1999; Liebske et al., 2005; Vetere et al., 2006; Del Gaudio et al., 2007]. At the lower viscosity end (<1 Pa s), represented by ultramafic melts, real time movies of the falling sphere are necessary and are obtained through the use of X-rays from a synchrotron source. At the upper viscosity end ($10^{4.5}$ Pa s), represented by granitic melts, the sinking distance of the sphere becomes smaller than its diameter and the sum of the experimental errors in determining the sphere location. Falling sphere viscometry has been employed at ambient [Dorfman et al., 1997; Riebling, 1966] and high-P conditions [e.g. Kushiro, 1978; Ryan and Blevins, 1987; Persikov et al., 1990; Scarfe et al., 1986; Dingwell, 1987; Brearley and Montana, 1989; and

White and Montana, 1990; Baker and Vaillancourt, 1995; Schulze et al., 1999; Liebske et al., 2005; Vetere et al., 2006; Del Gaudio et al., 2007] within piston cylinders and multi anvils [up to 130 kbar, Liebske et al., 2005] for simultaneous determination of density and viscosity. Maximizing the density contrast between the falling sphere and the surrounding melt reduces errors associated with the estimation of melt density and viscosity. Errors in density contrast can easily be reduced below the uncertainties inherent in the other variables affecting viscosity determination. Total errors for falling sphere viscosity determinations using the piston cylinder apparatus are probably nearer 20%. Burnham [1963] describes a variant on the falling sphere method in which the fall of a sphere, connected to a wire isolated electrically from the metal capsule, was electrically detected by the contact of the sphere against the capsule wall. Persikov et al. [1990] used a radioactive-tracer doped falling sphere in an internally-heated pressure vessel. The descent of the sphere is recorded radiographically as the sphere transits two "windows" in a lead shield. Very high pressure measurements of viscosity have been made by Kanzaki et al. [1987] who imaged the falling sphere in real time using a synchrotron radiation source. This method extends the lower limit of measurable viscosity using the falling sphere method at high pressure to 10^{-3} Pa s.

The highest viscosity that can be investigated by the falling sphere method may be expanded by the use of a centrifuge apparatus [Dorfman et al., 1996; Dorfman et al., 1997; Bagdassarov and Dorfman, 1998; Schmidt et al., 2006; Ardia et al., 2008]. With viscosity and acceleration scaling linearly, a centrifugal force of 1000g expands the viscosity range to 10^{7} Pa s. The elevated acceleration (up to 1000g) also allows investigating viscosities between the solidus and the glass transition temperature (T_g). This kind of measurements are commonly performed on pure liquids. I am aware of only one published paper [Vetere et al. 2010] which investigated multiphase rheology of andesitic lavas under pressure conditions. In a few cases these experiments were run at acceleration of 1000g by means of centrifuge falling-sphere methods [e.g. Ardia et al., 2008].

A1.4. PATERSON TYPE APPARATA

The gold standard for quantitative high pressure deformation studies is the gas apparatus developed by Paterson [1970] and Paterson and Olgaard [2000]. The apparatus can either compress or extend the sample. Some gas apparatus, for example, the Paterson gas apparatus [Paterson, 1970], can also deform the sample in torsion. Torsion allows much higher strains to be reached. Because the amount of strain in the sample varies radically from the centre to the edge in torsion experiments, torsion samples are constructed in the shape of a thin ring with jacket materials filling the centre. What gives the gas apparatus its edge is that the gas confining medium (usually Ar) provides a perfect uniaxial stress field. Because the gas supports no shear tractions along the sides of the sample or pistons, an external load cell can accurately measure the load supported by the sample. Unfortunately, the gas apparatus can only achieve a confining pressure of 500 MPa (5 kbar). This pressure is equivalent to the pressure at 15 km depth in the earth. The limited pressure range is a severe limitation for students of the deep earth. Online resources: an Introduction to High Pressure Rock Deformation Techniques can be found at:

https://serc.carleton.edu/NAGTWorkshops/mineralogy/mineral_physics/deformation_mechanisms.html.

A1.5. DIRECT VISCOSITY MEASUREMENTS ON ACTIVE FLOWS IN THE FIELD

Few direct measurements of lava rheology under natural conditions have been reported [Pinkerton and Sparks, 1978; Shaw et al., 1968; Belousov and Belousova, 2018; Chevrel et al. 2018]. Nonetheless, some of these methods are based on the assumption of a parabolic velocity profile (Jeffrey's eq) and have the limitations highlighted at paragraph 3.2.1. These measurements are crucial for benchmarking of experimental data, but insufficient to develop a systematic understanding of the evolution of lava-flow properties in response to varying external and internal parameters (composition, cooling-and shear-rate, oxygen fugacity etc.), as they represent snapshots of the system at one specific condition [Belousov and Belousova, 2018]. Belousov and Belousova, [2018] and Chevrel et al. [2018] present a review of of early studies as well as the most recent technological advances of this unique technique and new field measurement results. Such direct measurements in

the field require inserting a custom-built penetrometer, constituted by a steel bar with a half-spehrical penetration head [e.g. Belousov and Belousova, 2018], or a viscometer [Chevrel et al., 2018], into the molten lava while it is flowing. Such in-situ viscometry is challenging due to the difficulty of accessing an active lava flow, and the lack of appropriate instrumentation. Measurements under such conditions are therefore very restricted and have mostly been performed on slow advancing lava flows and far from the solidification point of the lava.

1) During penetration viscometry (similar to that used to perform micropenetration experiment in the lab), where a rod is pushed into the liquid lava, the force required to penetrate the lava is kept constant and penetration is monitored with time until penetration ceases. Viscosity of lava is then calculated based on Stoke's law for half a sphere (i.e. the half spherical penetrating tip of the penetrating rod). Belousov and Belousova [2018] employed the relationship proposed by Panov [1988], according to which:

$$\eta_S\ (Pa \cdot s) = \frac{F}{3\pi v \mathrm{R}} \qquad \text{(A1.7)}$$

where F is the force (N), v is the speed of penetration (m/s) and R is the radius of the penetration head (m).

2) The rotational viscometry method, requires a shear vane to be inserted into the molten lava and the shear stress values corresponding to various applied rotation rates is measured. Viscosity is estimated as the shear stress over the strain-rate ratio ($\eta = \frac{\tau}{\dot{\gamma}}$). The shear stress ($\tau$) is calculated by: $\tau = \frac{M}{2\pi h R_i^2}$ where M is the torque recorded by the torque sensor, h is the length of the vane and R_i is the equivalent radius of the rotating vane assuming a wide gap concentric cylinder geometry. The strain-rate ($\dot{\gamma}$) is calculated according to the following formula: $\dot{\gamma} = \frac{2\omega}{n\left[1-\left(\frac{R_i}{R_0}\right)^{\frac{2}{n}}\right]}$ where ω is the rotational velocity (rad/s) and R_i and R_o are the inner and the outer radius of the spindle. n is the flow index which is determined by performing measurements at various rotational speed. The advantage

of this approach is that it allows for evaluation of the lavas effective viscosity at a range of shear rates. Viscosity estimates obtained by employing this procedure are reported in Chevrel et al. (2018).

APPENDIX A2. EMPIRICAL AND THEORETICAL BASED FORMULATIONS TO EXPRESS THE T- AND P-DEPENDENCE OF THE VISCOSITY OF SILICATE LIQUIDS.

Among the known theoretical relations for coefficient of viscous flow of liquids, the Eyring arrhenian equation [Glasstone et al., 1941] is the most popular:

$$\eta = \eta_0 \exp(\Delta G/RT) \qquad (A2.1)$$

where R is the gas constant, T the absolute temperature and ΔG is the free activation energy of yield of the flow, that is, a function of the internal energy, entropy, P, and V (i.e. the volume of particles). The pre-exponential factor η_0, is related to the jump frequency of an atom from one structural site to another and represent the microscopic view of the "viscosity". It can be expressed as $\eta_0 = hN_A / V_m$) where h is the Planck's constant, ($6.63\ 10^{-34}$ J s), N_A the Avogadro's number ($6.02\ 10^{27}$) and V_m is the molar volume of the investigated liquid at very high temperature. This equation can be rewritten in logarithmic scale as it follows:

$$\log \eta = A + B/T \qquad (A2.2)$$

where $A=2.303*\log\eta_0$ and $B=\Delta G/R$. This Arrhenian form for viscosity has been used by Shaw (1972) and Bottinga and Weill (1972) to describe the first description of the viscosity of natural silicate melts.

Expansion of the melt viscometry database over a wider range of melt compositions and temperatures [closer to the so-called calorimetric glass transition temperature, T_g^{cal}, Angell, 1991; Scherer, 1984; Giordano et al., 2008a] exposed the limitations of Arrhenian models and new empirical and theoretical-based models have been provided to describe the temperature dependence of the viscosity of silicate liquids. In particular, the T–dependence of viscosity is accounted for by the three parameters in each of the most commonly employed formulation: (i) Vogel–Fulcher–Tamman (VFT) [Vogel, 1921; Fulcher, 1925; Tamman and Hesse, 1926]; (ii) Adam–Gibbs (AG)

(Adam and Gibbs, 1965) and (iii) Avramov (AV) (Avramov, 1998). These formulations accommodating the non-Arrhenian T -dependence of silicate melts, can be written as following:

$$\text{Vogel–Fulcher–Tammann (VFT):} \quad \log \eta = A_{VFT} + B_{VFT}/(T - C_{VFT}); \quad \text{(A2.3)}$$

$$\text{Adam and Gibbs (AG):} \quad \log \eta = A_{AG} + B_{AG}/[T\, S^{conf}(T,x)]; \quad \text{(A2.4)}$$

$$\text{Avramov (AV):} \quad \log \eta = A_{AV} + (B_{AV}/T)^{CAV}; \quad \text{(A2.5)}$$

where η is the viscosity in Pa s, T is the absolute temperature, and A, B, C, D and S^{conf} (T, x) [the so-called configurational entropy; representing the number of configurations accessible to the liquids at the glass transition (Tg), Richet, 1984] are adjustable parameters [e.g. Giordano and Russell, 2007; Giordano et al., 2008a, b; Russell and Giordano, 2017]. The literature shows that, in these systems, viscosity converges to a common value of the pre-exponential factors (A) that can be assumed, at fixed pressure, to be independent of composition [e.g. Russell et al., 2003; Russell and Giordano, 2005;; Giordano and Russell, 2007; Giordano et al., 2008a]. The other adjustable parameters in each equation are expanded to capture the effect of composition [Hui and Zhang, 2007; Giordano et al., 2008a]. Several other formulations exist that can be reconciled with the three model equations above mentioned. For instance, the most recent formulation of Mauro et al. [2009], which is based on the AG theory, assumes that S^{conf} (T) is closely connected with the topological degrees of freedom of atoms which provide an increased number of adjustable parameters. The most recent GRD and HZ models used to describe the viscosity of anhydrous and volatile bearing melts where B, C and S^{conf} parameters accommodate the effect of composition.

Empirical formulations used to constrain the effect of pressure on the viscosity of liquids and characteristic parameters of Equations (Eqs. A2.1-A2.5) are provided by various authors [e.g. Liebske et al., 2003; Ardia et al., 2008; Hui et al., 2009]. In particular, Liebske et al. [2003] by modelling the viscosity of andesitic magmas and Ardia et al. [2008] modelling the viscosity of more silicic magmas (rhyolites), used VFT expression (Eq. A2.3) where B_{VFT} parameter was function of H_2O and cubic and a linear function of P, respectively, and C_{VFT} parameter was only function of H_2O content and

independent of P. Fig. A2.1 reports, as an example, the variation of viscosity at constant T (1250 °C) as a function of P for melts of the Ab - Di system as fitted by using a linear dependence from P of the B_{VFT} parameter.

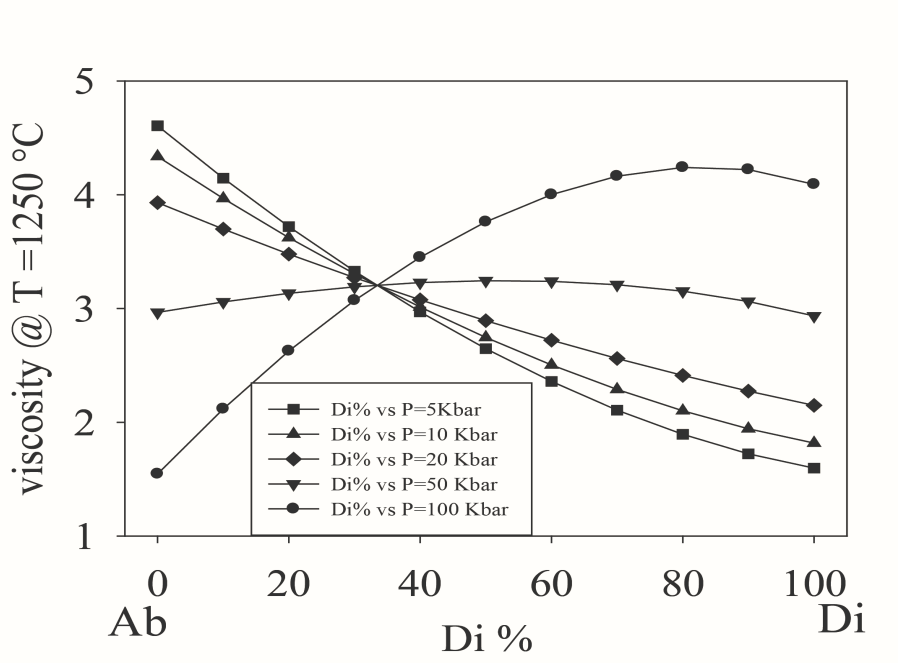

FIGURE A2.1. Isothermal viscosity variation as a function P (up to 100 kbar) for melts of the Ab-Di systems. The viscosity was calculated here using VFT equation (Eq. A2.3) where the B_{VFT} = B0, VFT +b1*P(Kbar), where B0, VFT is the pseudo-activation energy at 1 bar pressure and b1 is an adjustable parameter accounting for a linear P-dependence of B_{VFT}. The effect of composition is shown in the figure. At T=1250 °C the pure liquid viscosity of the albitic term (Ab100, left), proxy for a polymerized melt, is decreasing as P increases. On the other hand the pure liquid viscosity for the diopsidic melt (Di100, right), proxy for more depolymerized compositions, increases as P increases.

Online resources: a detailed summary of the philosophical approach employed to the construction of the GRD model, predictable variables and downloadable versions of the viscosity calculator can be found online at: https://www.eoas.ubc.ca/~krussell/VISCOSITY/grdViscosity.html

APPENDIX A3. EMPIRICAL FORMULATIONS TO EXPRESS THE EFFECT OF VARYING CRYSTAL/VESICLE CONTENT, SIZE AND SHAPE DISTRIBUTIONS AND STRAIN-RATE ON THE VISCOSITY OF MULTIPHASE MIXTURES.

Viscosity is defined as the resistance to flow under specific applied stress (σ) conditions and it is expressed by complex functions of applied stress and resulting strain (γ) and strain-rates (e.g., Herschel and Bulkley, 1926). For a Newtonian liquid, $\sigma = \eta\dot{\gamma}$ where η is the Newtonian viscosity. It is well-kown from both laboratory studies on analogue materials [e.g. Mueller et al., 2011; Cimarelli et al, 2011; Truby et al., 2015] and natural remelted volcanic rock [e.g Caricchi et al., 2008; Vona et al., 2011; Campagnola et al., 2016; Kolzenburg et al., 2016; Soldati et al., 2016, 2017] that suspended solids and natural crystals lead to the increase of the suspension's bulk viscosity of up to several orders of magnitude compared to the solid particles free counterpart. On the other hand the role of an addition of bubbles on a suspension may lead to both a viscosity increase (spherical bubbles) or decrease (oblate deformed bubbles) [e.g. Llewellin et al., 2002]. The presence of a solid phase or a gaseous phase to form a solid or bubble suspension commonly yield non-Newtonian behavior, expressed in the more general equation:

$$\sigma = \sigma_0 + K\dot{\gamma}^n \quad \text{(A3.1)}$$

where σ_0 is a stress threshold (or yield stress) to be overcome in order to start flow; *K* is the flow consistency (which corresponds to shear viscosity at γ = 1 s^{-1}) and *n* is the flow index which describes the degree of non-Newtonian behavior, being equal to 1 for Newtonian fluids, *n*>1 for shear-thickening and *n*<1 for shear-thinning fluids. For non-Newtonian fluid (σ_0=0), the term $\sigma/\dot{\gamma}$ is equal to $K\dot{\gamma}^{n-1}$ and an apparent viscosity will be defined as $\eta_{app} = \sigma/\dot{\gamma}$, while the relative viscosity (η_r)(ratio between stress and strain rate divided by the viscosity of the suspending liquid, η_l) will be expressed by:

$$\eta_r = \left(\frac{K}{\eta_l}\right) \dot{\gamma}^{n-1} \quad \text{(A3.2)}$$

where $K_r=K/\eta_l$ represents the relative consistency.

A3.1. BUBBLE-MELT SUSPENSIONS

When a bubble suspension flows bubble deformation is promoted, through the viscous forces, by shear (tending to deform bubbles) and opposed by surface tension which tends to restore/maintain bubble sphericity. The adimensional capillary number (*Ca*), i.e. the measure of the relative importance (i.e. the ratio) of shear and interfacial stresses, is: $Ca = \frac{\eta_{melt} \cdot r \cdot \dot{\gamma} \cdot}{\Gamma}$, where η_{melt}, r, $\dot{\gamma}$ and Γ are the viscosity of the suspension, the radius of the undeformed bubble, the shear rate of the flow and the liquid-vapour surface tension, respectively. The presence of bubbles can either increase or decrease the viscosity of a suspension depending on the dynamic regime [Manga et al., 1998; Lejeunne et al., 1999; Llewellin et al., 2002a,b; Rust and Manga, 2002; Stein and Spera, 2002; Llewellin and Manga, 2005]. Similar to solid particles, bubbles deform flow lines within the suspending medium, which tends to increase the viscosity. However, at the same time, they provide free-slip surfaces which favour flow. For $Ca<1$, interfacial tension forces dominate and bubbles are approximately spherical [e.g., Taylor, 1932]. In this case flow-line distortion is great and free-slip surface area is small, hence the overall effect is to increase the suspension viscosity. In contrast, at high deformation regimes, the bubbles will undergo significant elongation ($Ca>1$), thus favouring small flow-line distortion, greater free-slip surface area and a decrease in the suspension viscosity [Hinch and Acrivos, 1980, Llewellin and Manga, 2005; Vona et al., 2013, 2017].

However, the capillary number *Ca* implies an equilibrium between viscous and interfacial forces, and it can be applied only for steady flows, in which the conditions of shear have remained constant for a long enough time. As a consequence, if the shear strain rate is changing, the flow is unsteady and to describe unsteadiness Llewellin et al. [2002a, b] introduced the dynamic capillary number $Cd = \frac{\eta 0 \cdot r \cdot}{\tau} \frac{\ddot{\gamma}}{\dot{\gamma}}$, where the double derivative of strain-rate is the speed of strain-rate variation. For $Cd \ll 1$, the changes in shear environment are slow enough to allow the bubbles to reach their equilibrium shape, hence flow is steady and the dynamic regime is controlled by the capillary number

Ca. On the other hand, if *Cd*≫1, flow is unsteady, the bubbles are not able to reach their equilibrium shape in response to fast strain rate and they are, therefore, unrelaxed (they are actively deforming). In other words, in these conditions the rate of bubble deformation is large compared with the bulk strain rate and, therefore, most of the strain is accommodated by deformation of the gas in the bubbles. Since the gaseous phase has a negligible viscosity, this leads to a decrease of viscosity as the bubble content increases. Llewellin and Manga [2005] parameterized the effect of bubbles on the relative viscosity of a bubbly suspension, considering a single equation for the positive dependence of ηr on ϕb and a single equation for the negative dependence of ηr on ϕb, regardless of whether the decrease in viscosity in the latter case is related to steady (*Ca*>1) or unsteady (*Cd*>1) flow. Based on existing literature models [Bagdassarov and Dingwell, 1992, 1993; Pal 2003, Llewellin et al., 2002a,b], the authors suggested two different parameterizations for each viscous regime (increasing and decreasing η_r), considering two limiting cases corresponding to a minimum (MIN) and a maximum (MAX) effect of the bubbles on the viscosity of the suspensions.

For Ca<1 (increasing η_r):

$\eta_r=(1-\phi_b)^{-1}$ (MIN: Pal 2003); $\eta_r=(1+9\phi_b)$ (MAX: Llewellin, 2002a,b) (A3.13)

For Ca>1 or Cd>1 (decrasing η_r):

$\eta_r=(1-\phi_b)^{5/3}$(MIN: Pal 2003); $\eta_r=[1/(1+22.4\phi_b)]$ (MAX: Bagdassarov & Dingwell, 1992) (A3.14)

Online resources: a synthesis of the results obtained by Llewellin research can be found at the following webpage: http://community.dur.ac.uk/ed.llewellin/rheology.htm

Quane and Russell [2005], Russell and Quane [2005] and Robert et al. [2008a, b] by performing uniaxial compression experiments on porous samples modelled the effective evolving viscosity (η_e) and porosity (φ) as from Russell and Quane [2005]:

$$\log \eta_e = \log \eta_0 - [\alpha\varphi/(1-\varphi)]^{\beta} \quad \text{(A3.15)}$$

where α, β are unknown adjustable coefficients and η_o is the unknown effective viscosity of the melt plus crystal cargo at zero porosity. The parameter β was added to the original model of Ducamp and Raj [1989] to capture the full range of data and preserve a concave down equation form in the variables space (η, φ). The employed model was used to estimate the timescale for the welding of the block and ash flow deposits at Mount Meager. The results of the specific measurements of Quane and Russell [2005], Russell and Quane [2005], Robert et al [2008a, b] and new data on natural samples were compared by Vona et al. [2016] with the modelling proposed by Mader et al [2013], based on the analysis of analogue materials. Those results are in better agreement with the model proposed by Bagdassarov and Dingwell [1992]. Finally, Vona et al. [2016] proposed a model to evaluate the strength of vesiculated magmas based on Eq. A3.15.

A3.2. CRYSTAL-MELT SUSPENSIONS

In the last decades a significant number of experimental studies have investigated the rheological properties of different solid-bearing suspensions constituted by synthetic analogues [Mueller et al., 2011; Cimarelli et al., 2011; Moitra and Gonnermann, 2015; Truby et al., 2015; Klein et al., 2017, 2018; Dobson et al., 2015, 2016]; synthetic silicate melts [Lejeune and Richet, 1995; Caricchi et al., 2007; Champallier et al., 2008 and Costa et al., 2007a, 2009] and crystal-bearing natural magmas at subliquidus temperatures [e.g., Gay et al., 1969; Shaw, 1969; Marsh, 1981; Ryerson et al., 1988; Pinkerton and Stevenson, 1992; Pinkerton and Norton, 1995; Sato, 2005; Ishibashi and Sato, 2007; Caricchi et al., , 2008; Ishibashi, 2009; Vona et al., 2011, 2017; Campagnola et al., 2016; Kolzenburg et al., 2016, 2017, 2018].

In crystal-melt suspensions, the dispersed phase acts as a ‘hard’ (non-deformable) inclusion which increases the viscosity of the suspension through both hydrodynamic and mechanical interaction among crystals. For low solid fractions, the viscosity increases slowly with the particle volume fraction (ϕ), and the suspension maintains a Newtonian rheological behavior (strain-rate independent). When ϕ exceeds a critical value (ϕ_c), particles start to interact with each other and a

solid network of particles begins to form, causing a strong increase in viscosity and the onset of non-Newtonian flow, characterized by Bingham-like rheology and/or shear thinning effects (Eq. 1). As the solid fraction is further increased, the system reaches another rheological threshold, corresponding to the maximum packing density of solid particles (ϕ_m) Figure 2), which causes the transition from melt and melt+crystal to solid-state creep rheology [e.g., Kohlstedt and Zimmerman, 1996; Lavallée et al., 2007, 2008, 2012]. The value of ϕ_c is defined by both the crystal content as well as by the crystal size and crystal shape distributiosn [e.g. Costa et al., 2009; Cimarelli et al., 2011; Vona et al., 2011]. The increase in viscosity and the non-Newtonian flow depend on textural features (crystal and bubble distribution) and deformation regimes [e.g., Costa et al., 2009; Petford, 2009; Mueller et al., 2011].

A number of models have been proposed describing the effect, on the suspensions rheology, of the crystal volume fraction and their,shape and size distributions as well as particles roughness and deformability [e.g., Einstein, 1906; Roscoe 1952; Maron and Pierce, 1956; Krieger and Dougherty, 1959; Frankel and Acrivos, 1970; Jeffrey and Acrivos, 1976; Marsh, 1981; McBirney and Murase, 1984; Costa, 2005; Hsueh and Becher, 2005; Stickel and Powell, 2005; Caricchi et al., 2007; Champallier et al., 2008; Costa et al., 2009; Ishibashi, 2009; Mueller et al., 2011; Cimarelli et al., 2011; Vona et al., 2011, Mader et al., 2013; Moitra and Gonnermann; 2015; Klein et al., 2017, 2018]. The various models can be applied to represent the viscosity variation from a dilute ($\phi<0.03$, where viscosity increase is linear with crystal content and it is Newtonian) to a semi-dilute ($\phi<0.25\text{-}0.40<\phi_c$, where viscosity shows an increasing dependence of crystal fraction, but it is still Newtonian) until a concentrated regimes ($\phi_c<\phi<\phi_m$, for which viscosity shows a rapid increase and the onset of non-Newtonian rheology). For $\phi>\phi_m$ a solid creep-dominated rheology is observed until the occurrence of brittle failure. The crystal fraction ϕ at the transition between one and the other regime depends strongly from the shape and size distributions [e.g. Saar et al., 2001; Costa et al., 2009].

So far, one of the most comprehensive models describing the relative viscosity variation from dilute to highly concentrated regimes is that proposed by Costa et al. (2009)(CM). According to that model:

$$\eta r(\phi) = \frac{1+\varphi^{\delta}}{[1-F(\varphi,\xi,\gamma)]^{B\phi^*}} \quad \text{(A3.3)}$$

where

$$F = (1-\xi)erf\left[\frac{\sqrt{\pi}}{2(1-\xi)}\varphi(1+\varphi^{\gamma})\right] \quad \text{(A3.4)}$$

with $\varphi = \phi/\phi^*$ where ϕ^*, ξ, γ and δ are adjustable parameters that depend on the deformation rate (Costa et al., 2009) and B is the Einstein coefficient (Einstein, 1906). The parameter ϕ^* represents the critical solid fraction at which the rheological transition from a dominant liquid phase regime switches to a regime where the effect of crystals is predominant and the viscosity values are much higher [Costa, 2005; Costa et al., 2009]. The CM is calibrated using suspensions containing crystal fractions, isotropically distributed, in the interval ϕ = 0.1 - 0.8.

Figure A2.1 shows, based on the Costa et al. [2009] model (CM), the strain-rate dependence of the relative viscosity at varying crystal volume fractions. The relative viscosity of two-phase mixture increases following a sigmoid curve with exponential increase above a critical solid fraction (ϕ_c), corresponding to the first inflection point in Figure 2. This documents how variations of crystal content may cause orders of magnitude changes in suspension viscosity. A further important point in models of suspension rheology is that the maximum critical crystal volume fraction (ϕ_m) depends strongly on crystal shape, size distribution, crystal surface roughness and crystal orientation [e.g. Mueller et al., 2011; Mader et al., 2013; Klein et al., 2017; 2018]. In general, ϕ_c and ϕ_m decrease with increasing crystal alignment and particle shape anisotropy (i.e., equant vs elongated) and increases with dispersion in object size and surface roughness [e.g. Chong, 1971; Lejeune and Richet, 1995;

Saar et al., 2001; Caricchi et al., 2007., 2008; Costa et al., 2009; Vona et al., 2011; Mueller, 2011; Mader et al., 2013; Klein 2018].

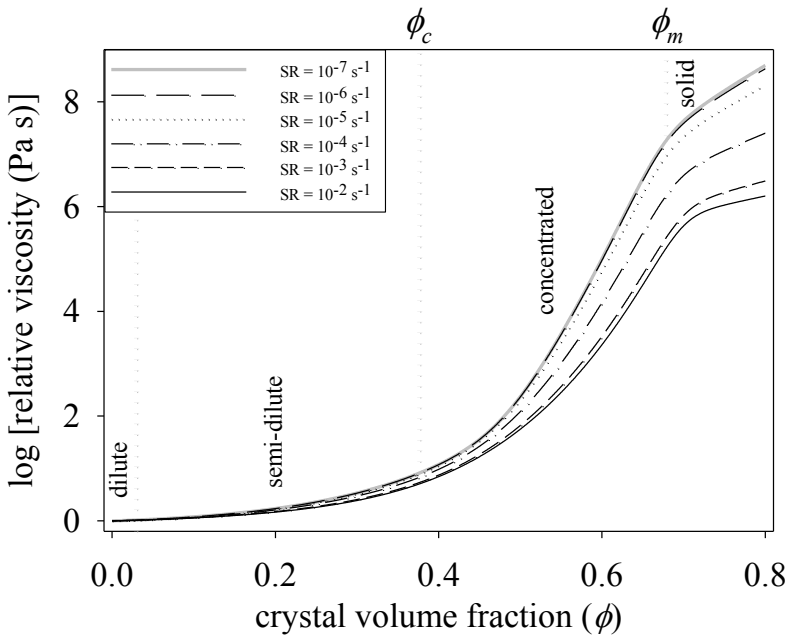

FIGURE A.2.1. **(a)** Relative viscosity as a function of crystal volume fraction of spheres at different strain-rates as calculated with the Costa et al. (2009) model. The figure shows, at first approximation, the inflection points at ϕ_c and ϕ_m, separating the semi-dilute, concentrated and solid-like deformation regimes and the dilute regime as described in the text. The inflection points are a function of the applied shear rates and shape and size distributions.

Mueller et al. [2011] by studying the rheological response of monodisperse suspensions with different aspect ratios, and adopting the Maron-Pierce equation, where

$$\eta_r = \left(1 - \frac{\phi}{\phi_m}\right)^{-2} \qquad \text{(A3.5)}$$

concluded that both the flow index n and (Eq A3.1) the critical crystal fraction depend on the average particle aspect ratio (R), such that:

$$n = 1 - 0.2R\left(\frac{\phi}{\phi_m}\right)^4 \qquad \text{(A3.6)}$$

where the dependence of the ϕ_c from R-parameter is given, as in Mueller et al. [2011] by:

$$\phi_m = \frac{2}{0.321R + 3.02} \qquad \text{(A3.7)}$$

It is worth mentioning that the parameterization of Mueller et al [2011[and Mader et al. [2013] cannot extended above the critical solid fraction ϕ_m.Other authors [e.g Ishibashi, 2009; Mueller et al., 2011; Vona et al., 2011] proposed parameterizations obtained by modifications of the strain rate independent KD equation [Krieger and Dougherty, 1959]

$$\eta_r = \left(1 - \frac{\phi}{\phi_m}\right)^{-B\phi_m} \quad \text{(A3.8)}$$

to take into account the shear thinning effect on the rheology of suspensions. These authors provided modified strain rate dependent KD equations based on rheological measurements on low SiO_2 melts. Ishibashi (2009) provided the following expression for the relative viscosity:

$$\eta_r = \left(1 - \frac{\phi}{\phi_m}\right)^{-B_1\phi_m[1+\lambda\, ln(1-\phi/\phi_c)ln\dot{\gamma}]} \quad \text{(A3.9)}$$

where ϕ_m = 0.6 (as in the ER equation), B_1 = 5.46 represents the intrinsic (melt) viscosity at $\dot{\gamma}$ =1 s^{-1} and λ = 0.118 is an empirical constant which takes the shear thinning effect into account. In the Ishibashi (2009) parameterization, the fitting parameters were not related to the textural features of the suspensions (e.g., crystal shape, crystal shape dispersion, crystal size dispersion and orientation dispersion), such that the parameterization cannot be applied to other suspensions.

Later, Cimarelli et al. [2011] by using a KD expression extended the application of the parameterization provided by Mueller et al. [2011] to account for bimodal shape polydispersion of particles.

Finally Vona et al. [2011] on the basis of rheological measurements on crystallizing polydispersed crystal-rich basalts provided a similar KD-derived parameterization

$$\eta_r = \left(1 - \frac{\phi}{\phi_m}\right)^{-2[1-\alpha log(\dot{\gamma})]} \quad \text{(A3.10)}$$

in which α is an empirical parameter equal to 0.06 and the effect of crystal shape can be evaluated using the equation proposed by Mueller et al. [2011] (Eq. 9) where, in order to account for

the disperse particle size distribution of the natural samples investigated, the average particles ratio ($\overline{R}$) is calculated by averaging the contribution of each group of particles having a certain aspect ratio and is called as it follows:

$$\bar{R} = \frac{\sum \phi_i \bar{R}_i}{\phi} \quad \text{(A3.11)}$$

where ϕi and $\overline{R}_i$ are the crystal fraction and the mean aspect ratio of phase *i*. The model by Vona et al. (2011) is able to describe the rheological behavior of suspensions as a function of strain rate and textural features (i.e., crystal fraction, aspect ratios and shape polydispersion) and can be therefore applied to the complexities of natural magmas. An additional step ahead is provided by the work of Klein et al (2017, 2018) which express the critical crystal aspect ratio (ϕ_c) as a function of a polydispersity parameter (χ)(γ in Klein et al., 2018):

$$\phi_c = 1 - (1 - \phi_{c,0})\, \chi^{\alpha} \quad \text{(A3.12)}$$

where $\phi_{c,0}$ represents the ϕ_c for a unimodal distribution of particles and α is an adjustable parameter (α = 0.173). The polydispersity employed is the ratio of the specific surface of a polydispersed system and that of a monodisperse system [Torquato, 2013; Wadsworth et al., 2017]. Klein and coauthors employing Maron-Pierce kind of equation (Eq. A3.5) to express the relative viscosity and the parameterization of Mueller et al [2011] to account for the crystal ratio obtain and interesting expression for the relative viscosity of a polydisperse suspention and provide as supplementary material online an user-friendly spreadsheet .to calculate such a value [https://doi.org/10.1016/j.jvolgeores.2018.04.018].

A3.3. THREE PHASE MIXTURES

Only few studies have explored the rheology of crystal and bubble-bearing magmas [e.g. Cordonnier et al., 2009; Pistone et al. 2012, 2013; 2015, 2016; Campagnola et al., 2016; Plese et al., 2018]. Lavallée et al. [2007], Avard and Whittington [2011] have investigated natural lavas from domes by uniaxial deformation experiments. The authors have observed pseudo-plastic behavior with

a strong shear thinning component for all the investigated magmas and provided equations describing the apparent viscosity as a function of temperature and strain rate for the multiphase magmas. Pistone et al. [2012] showed that three crystal and vesicle contents domains where non-Newtonian rheological behaviour varying from shear thinning (e.g. viscosity decreases as strain-rate increases and the flow index n < 1, Eq. A3.1) to shear thickening (e.g. viscosity increases as strain-rate increases and the flow index n > 1, Eq. A3.1) through intermediate between shear thickening and shear thinning were observed. The authors concluded that shear thinning occurred in crystal-rich suspensions (55-65 vol%) and bubble content of 9-10 vol% as due to crystal size reduction and shear localization. Shear tickening was instead observed in dilute suspensions (24 vol% crystal content, 12 vol% bubbles) as due to bubbles coalescence and boudinage which favoured water loss from the melts and sample degassing. Intermediate behaviour was observed for samples with 44 vol% crystals and 12 vol% bubbles probably due to the different temperatures and the time of experiments which did not give always time to the bubbles and crystal to orient along the flow lines, passing from prolate to oblate. The authors also showed that, caused by crystals and bubbles interactions, the interactions between flow-lines and crystals plus bubbles cannot be compared to that occurring for crystals and bubbles in only two-phase suspensions. Results from Pistone et al. [2012] were applied to understand the process of viscous death and rejuvenation of magmatic bodies stored at depth [e.g. Bachmann and Bergantz, 2006].

The individual effect of crystal and bubbles was theoretically parameterized by Phan-Thien and Pham [1997] and later applied by Harris and Allen [2008] for the study of basaltic magmas from Mauna Loa and Mount Etna. Depending on the relative size of crystals ($\Phi_{xtl,\,tot}$) and vesicles (Φb), Phan-Thien and Pham [1997] present three equations:

1. For crystals smaller than vesicles:

$$\eta = \eta_l \left(1 - \frac{\phi_{xtl,tot}}{1-\phi_b}\right)^{-\frac{5}{2}} (1-\phi_b)^{-1} \qquad \text{(A3.16)}$$

2. For crystals and vesicles of equal size:

$$\eta = \eta_l \left[1 - \phi_{xtl,tot} - \phi_b\right]^{\frac{\left(-5\Phi_{xtl,tot}+2\Phi_b\right)}{\left(2\left(\Phi_{xtl,tot}+\Phi_b\right)\right)}} \quad \text{(A3.17)}$$

3. For crystals larger than vesicles:

$$\eta = \eta_l \left(1 - \frac{\phi_b}{1-\phi_{xtl,tot}}\right)^{-1} \left(1 - \phi_{xtl,tot}\right)^{-\frac{5}{2}} \quad \text{(A3.18)}$$

This treatment does not take into account the effect of textural variability, being applicable to spherical particles only, and strain rate dependency on the rheology.

APPENDIX A4. EQUATIONS TO ESTIMATE RHEOLOGICAL PROPERTIES OR CONSTRAIN CHARACTERISTIC FLOW LAWS PARAMETERS STARTING FROM FIELD OBSERVATION OF THE GEOMETRICAL FEATURES OF LAVA FLOWS.

Where direct measurement of the viscosity of lava flows (see A1.5) is not accessible the most accurate method to estimate the viscosity of lava flows is the so-called flow rate method [e.g. Kolzenburg et al., 2017, 2018a; Belousov and Belousova, 2018]. Measuring accurately the flow rate of active lava flows allows calculating the apparent viscosities of the lava flows using Jeffreys' equations:

$$\eta = \rho g h^2 * \frac{sin(\alpha)}{3v} \textit{ (Eq. A4.1); } \eta = \rho g h^2 * \frac{sin(\alpha)}{2v} \quad \text{(A4.2)}$$

where η is the viscosity of lava (Pa s), ρ is the bulk density (kg/ m3), g is the gravitational acceleration (9.8 m/s2), h is the thickness of the lava flow (m), α is the surface slope (degrees), and v is the velocity of lava flow (m/s). Eq. A4.1 is commonly used for data observing the flow front velocity, and the Eq. A4.2 is used for velocity observations of the flow surface behind the flow front (e.g. Nichols 1939; Gauthier 1973; Panov et al. 1988; Belousov nd Belousova, 2018]. Measurements using this procedure are reported in several studies [e.g. Nichols 1939; Minakami 1951; Macdonald 1963; Einarsson 1966; Walker 1967; Gautier 1973; Andreev 1978; Fink and Zimbelman 1986; Vande-Kirkov 1987; Moore 1987; Panov 1988; Soldati 2016]. Limitations of Jeffrey's equations have been discussed at 3.1.2.

Lava flow morphologies are thought, under particular assumptions, to reflect the rheological characteristic of the lavas [e.g., Wilson and Head, 1983; Hiesing et al., 2007]. Assuming that: i) the rheological properties can be estimated from remote sensing data; ii) the geometry of the flow depends on lava rheology and that lava behaves as a Bingham fluid (i.e. a fluid whose rheological law is expressed by $\tau = \tau 0 + \eta * \dot{\gamma}$; where τ is the shear stress and τo is yield strength, that is, the shear stress necessary to first determine the beginning of the flow); iii) no inflation of the lava has occurred; then the yield strength of the lava flow (Pa) and the lava flow viscosity can be related to its geometry

according to the equations proposed by Moore et al. [1978]. These equations, commonly employed in planetary science, have been recently adopted in numerous scientific contributions which also provide exhaustive reviews of the present state of art for the application of this method [e.g. Hiesinger et al., 2007; Chevrel et al., 2015; Castruccio et al., 2010, 2014; Kolzenburg et al., 2018a amongst the others]. These contributions together with the new advances, due to comprehend the effect of crystalline and bubbles phases on the rheology of multiphase lavas, pointed out that this method, given the strong constitutive assumptions (in particular, single value of viscosity and yield strength during lava field evolution and emplacement), are not accurate enough to be employed, for instance, for real-time monitoring of lava flows [Chevrel et al., 2015].